IEEE Access
Multidisciplinary | Rapid Review | Open Access Journal

Received April 5, 2020, accepted April 16, 2020, date of publication April 27, 2020, date of current version May 14, 2020.

Digital Object Identifier 10.1109/ACCESS.2020.2990729

Coordinated Chassis Control of 4WD Vehicles Utilizing Differential Braking, Traction Distribution and Active Front Steering

JIANBO FENG, SIZHONG CHEN, AND ZHIQUAN QI
Beijing Institute of Technology, Beijing 100081, China

Corresponding author: Zhiquan Qi (qizhiquan@bit.edu.cn)

This work was supported by the National Key R&D Program of China: under Grant 2017YFB0102600. The work of Zhiquan Qi was supported by APC.

ABSTRACT This paper proposes a coordinated chassis control (CCC) utilizing four-wheel differential braking, electronically controlled real-time four-wheel drive (4WD) and active front steering (AFS), aiming to improve the driving performance and handling stability during cornering. First, the performance of the single system is tested; then the hierarchical-structure control algorithm is designed: a supervisory controller to monitor vehicle states and determine the desired yaw rate, upper-level controller to decide the desired longitudinal forces and the desired yaw moment based on the driver intention and the consideration of vehicle stability, and the control allocation layer to distribute the actual control inputs to the actuators applying an optimal control allocation algorithm. Simulations of moderate driving/aggressive deceleration scenarios and a comprehensive test on a handling road are conducted to validate the effectiveness of the proposed control algorithm. The results of the simulations suggest that the proposed algorithm can effectively improve the driving speed in limit cornering without losing lateral stability, and reduce the tire dissipation energy compared with other control algorithms such as the electronic stability control system, the four wheel independent brake system and an integrated chassis control system proposed in a previous research.

INDEX TERMS Coordinated chassis control, tire dissipation energy, limit handling, vehicle dynamics.

NOMENCLATURE

v_x	Vehicle longitudinal velocity.
$\bar{v}_x$	Estimated vehicle longitudinal velocity.
v_{target}	Target vehicle longitudinal velocity.
v_y	Vehicle lateral velocity.
δ_f	Front wheel steering angle.
γ	Yaw rate.
γ_{des}	Desired yaw rate.
γ_{Target}	Target yaw rate.
m	Total mass of the vehicle.
l_f, l_r	Distance from center of gravity to front/rear axle.
l	Wheel base.
F_{xii}	Longitudinal forces of the front/rear wheels, $ii = fl, fr, rl, rr$.
F_{yii}	Lateral tire forces of the front/rear wheels.
F_{zii}	Vertical tire forces of the four wheels.
$\bar{F}_{xf}$, $\bar{F}_{xr}$	Overall longitudinal forces in front/rear axle.
$\bar{F}_{yf}$	Overall lateral force in front axle.
I_z	Yaw moment of inertia about the z-axis.
t_w	Tread (track width).
F_T	Traction force induced by 4WD.
F_B	Brake force induced by ESC.
T_{eng}	Output drive torque of the engine.
T_{trans}	Output torque of the transmission.
T_{4WD}	Total drive torque of 4WD system.
T_{f-4WD}	Drive torque of 4WD system in front axle.
T_{rl-4WD}, T_{rr-4WD}	Drive torque of 4WD system in rear-left and rear-right wheel, respectively.
a_x	Longitudinal acceleration.
a_y	Lateral acceleration.
$a_{y,\max}$	Maximum lateral acceleration based on the curvature of the path.
I_{yaw}	Yaw motion understeer index.
γ_{des}	Desired yaw rate.
$\gamma_{\max}$	Maximum yaw rate.

The associate editor coordinating the review of this manuscript and approving it for publication was Shihong Ding.

μ	Road-tire friction coefficient.
g	Gravitational acceleration constant.
$K_{p-f/r}$	Tuning parameter for front/rear traction torque ratio of 4WD.
$K_{p-l/r}$	Tuning parameter for left/right traction torque ratio in the rear axle of 4WD.
ω_f, ω_r	Rotational speed of the input/output shaft of the center coupling.
I_{cc}	Current input for the center coupling.
$T_{F,4WD}$, $T_{R,4WD}$	Drive torque distributed to the front/rear axles by the center coupling, respectively.
δ_{driver}	Steering wheel angle by the driver.
δ_{AFS}	Steering wheel angle by AFS.
$C_{\alpha f}$, $C_{\alpha r}$	Front/rear tire cornering stiffness.
$F_{xii,ESC}$	Longitudinal tire forces generated by ESC, ii = FL, FR, RL, RR.
$F_{xii,4WD}$	Longitudinal tire forces generated by four-wheel drive (4WD).
v	Vehicle combined speed.
α_f, α_r	Slip angle of the front/rear tire.
β	Vehicle sideslip angle.
M_z	Yaw moment.
r	Effective rolling radius of the wheels.
$\delta_{f,\max}$	Upper limit of front wheel steer angle.
$\alpha_{f,\max}$	Upper limit of the front wheel slip angle.
$p_{\max}$	Upper limit of the M/C pressure.
ξ_{u1}, ξ_{v2}, ξ_{v3}	Weighting factors on cost functions.

I. INTRODUCTION

Vehicles tend to be more over-actuated nowadays with more and more independent control modules/systems mounted, in order to improve the lateral safety and driving comfort of the drivers and passengers. The most mentioned and assessed longitudinal/lateral/vertical systems in literatures are Four Wheel Drive (4WD), Active Front Steering (AFS), Rear-wheel steering (RWS), Electronic Stability Control (ESC), active roll control system (ARCS), and active suspension system [1], [2], etc. With the increase of the number of the chassis modules mounted on the vehicle, the development of the coordinated control algorithm of the modules has been a hot research topic.

The integration of multiple modular chassis control systems can provide more economic and efficient performance than the traditional individual control systems, as is shown in many literatures.

Several literatures contribute research efforts to the integration of active steering and differential braking with different control allocation approaches. A simple coordination of steering and individual wheel braking has been proposed to enhance vehicle yaw stability control [3], which demonstrates the effectiveness of the integration of different control modules. An optimum yaw moment distribution with AFS and ESC utilizing an adaptive tuning rule and taking the physic limit into consideration was proposed [4], in which the weighted pseudo-inverse-based control allocation was utilized to solve the optimal control allocation problem. Goodarzi *et al.* [5] took advantage of active steering control (ASC) and direct yaw-moment (DYC) to control the vehicle path tracking automatically, in which feedback/feedforward methods were adopted. Yim [6], [7] proposed two unified chassis control systems of ESC and AFS for the under-steer prevention induced by the use of AFS in lateral motion and improved vehicle stability performance, respectively. The intuitive advantage of the integration of active steering and differential braking lies in that, in moderate driving scenario, AFS can handle the mild external disturbances and modify the driver's steering input to optimize the vehicle's lateral performance [8]–[10], and in high speed turning scenario, ESC will step in to decelerate the vehicle and, combined with AFS, produce the desired yaw moment.

Other researches have focused on the integration of some other chassis control modules. March and Shim [11] proposed an integration of active controlled suspension system and the front steering to improve the vehicle safety and lateral performance. Guo *et al*. [12] investigated the trajectory tracking of autonomous vehicles using the integration of 4WD and ESC, which considered the highly coupling effects of the vehicle and tire dynamics, and used a back-stepping sliding mode controller to decide the desired longitudinal/lateral forces. Joa *et al*. [13] presented an integrated chassis control of front/rear 4WD and differential ESC, to improve the performance in normal driving and limit handling combined, in which a tire dissipation energy (TDE) and tire longitudinal/lateral combined slip-based cost function was proposed to calculate the desired virtual control input. Her *et al*. [14] proposed an integration of three chassis modules: front/rear 4WD, ESC and ARCS, in the paper the 4WD system can generate the desired longitudinal acceleration while ESC is used to produce the desired yaw motion in steering scenario and ARCS can help manage the vertical load of every tire, which can expand the friction circle of every tire to a larger scale to enhance the lateral handling. In these researches, integration of different chassis control systems has been the main topic. The main difference of this paper from the previous research is that, the coordinated chassis control system proposed in this paper consists of driving (4WD) and braking (four-wheel independent braking), longitudinal dynamics control and lateral dynamics control (AFS), and by use of appropriate allocation algorithm the control effect theoretically should be better than individual control systems and the simple integration of the individual control systems.

In this paper, we propose a coordinated chassis control (CCC) system of 4WD, AFS and four-wheel independent braking system, to enhance both longitudinal and lateral motions of the vehicle, which makes the vehicle faster in straight driving and more stable in cornering occasions. The algorithm is comprised of three layers: the supervisory layer to monitor the vehicle states and calculate the desired yaw

rate; the upper-level layer to decide the desired longitudinal forces and the target yaw moment, the tire force control allocation layer to distribute the optimized tire forces and steering angle to the actuators to match virtual control inputs. The rest of the paper will be organized as follows, first, the system dynamics based on the planar dynamics model will be presented; then, the control algorithm of the individual chassis module will be given based on previous researches; Following that, a coordinated chassis control algorithm will be designed with the integration of the three control modules based on the optimized control allocation method; finally, the performance of the proposed control algorithm will be verified through Matlab/Simulink and Carsim co-simulation with comparison to other control systems, and some conclusions will be made.

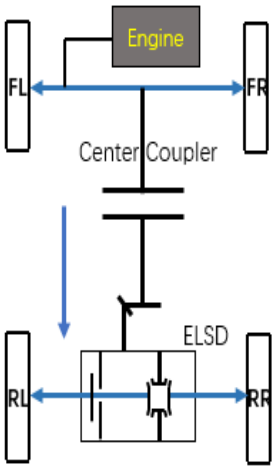

FIGURE 1. Vehicle driveline configuration.

II. CHASSIS SYSTEM DYNAMICS

A. VEHICLE DYNAMICS MODEL

The 4WD based vehicle configuration is shown in Fig. 1, the vehicle is mounted with a electromagnetically controlled center coupler and an electronically controlled limited slip differential (ELSD), enabling the driving torque to be transferred from front to rear axle and left to right in the rear axle. The vehicle dynamics during cornering is illustrated with a planar model as in Fig. 2. The dynamics equations of the system can be expressed by equation (1), as shown at the bottom of the next page. The modification term of the lateral force ΔF_{yii} corresponds to $\Delta\delta_f$ generated by AFS in the control allocation layer, both of which will be discussed in following sections. This kind of configuration of 4WD can enhance the lateral motion performance when the vehicle accelerates compared with the simple front/rear traction distribution 4WD system [15].

In the proposed chassis control algorithm, the constrained front/rear and left/right traction forces from 4WD, 4-wheel-independent braking from ESC and auxiliary front steering from AFS are utilized to optimize the control of the vehicle.

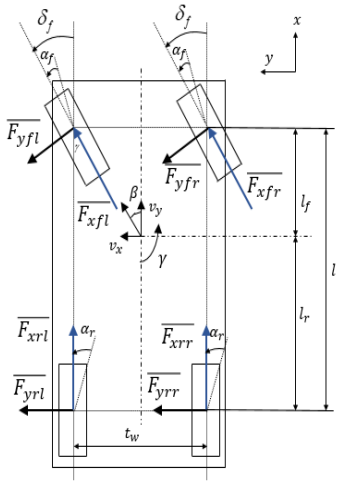

FIGURE 2. Planar dynamics model.

B. THE INDEPENDENT CONTROL OF THE CHASSIS MODULES

The control effect of the individual chassis module is shown in Fig. 3. AFS, as a device that can change the lateral force of the front wheels by steering the front wheels, acts as the direct control method of the yaw motion; While the two longitudinal direction modules, 4WD and ESC, can have both direct control and indirect control effects simultaneously, in that, by differential driving or braking, they can induce yaw moment directly through longitudinal tire forces, then according to the friction circle limit of the tire forces, the existing coupling correlation between lateral tire forces and longitudinal forces can induce corresponding changes of the yaw moment with the variation of the longitudinal force (F_x).

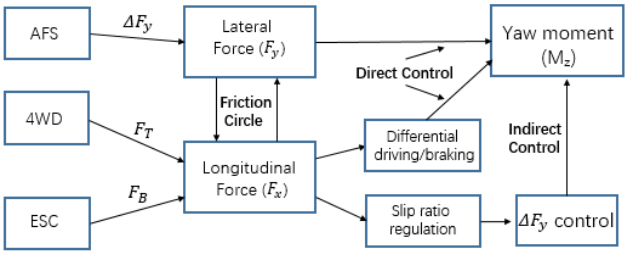

FIGURE 3. The control effects of the chassis modules in cornering scenario.

The performance of the proposed integration algorithm will be validated through the comparison with the individual module controllers, thus, the performance of each of the three modules controllers will be addressed in the following section.

1) DRIVING TORQUE DISTRIBUTION (4WD)

The driving distribution module is controlled to meet the driver's demand to achieve the desired longitudinal velocity in straight-line driving and desired yaw motion in cornering. For straight-line driving, the target longitudinal acceleration can be calculated from the indicated engine output torque

which is originated from the acceleration pedal input by the driver and received by the controller via CAN (Controller Area Network) Bus.

$$a_{xt} = f(T_{eng}) \tag{2}$$

Then the overall drive torque distributed by 4WD system can be determined by,

$$T_{4WD} = T_{f-4WD} + T_{rl-4WD} + T_{rr-4WD} = m \cdot a_{xt} \cdot r \tag{3}$$

Other than the longitudinal acceleration requirements, the torque distribution also need to satisfy the need to enhance yaw motion control, which can be managed by a certain yaw motion performance index I_{yaw} determined as follows [14],

$$I_{yaw} = \frac{(\gamma_{des} - \gamma)}{\gamma_{\max}} \cdot \mathrm{sgn}(\gamma) \tag{4}$$

where, $I_{yaw} > 0$ when the vehicle is in understeer state, and $I_{yaw} < 0$ when the vehicle oversteers. The maximum yaw rate in the equation in condition of nice dry asphalt road can be given as follows [16],

$$\gamma_{\max} = 0.85\frac{\mu g}{V_x} \tag{5}$$

Then, satisfying the overall longitudinal driving force, the desired 4WD distribution and the actual control input of the 4WD system can be determined based on the dynamic modeling of the center coupler and ELSD, as in equation (6)-(8).

$$T_{f-4WD} = 0.5 \cdot T_{4WD} - \frac{K_{p-f/r}}{2} \cdot I_{yaw} \tag{6}$$

$$T_{rl-4WD} = 0.25 \cdot T_{4WD} + (\frac{K_{p-f/r}}{4} - \frac{K_{p-l/r}}{2}) \cdot I_{yaw} \tag{7}$$

$$T_{rl-4WD} = 0.25 \cdot T_{4WD} + (\frac{K_{p-f/r}}{4} + \frac{K_{p-l/r}}{2}) \cdot I_{yaw} \tag{8}$$

The internal structure of center coupling is shown in Fig. 4. It consists of two sets of clutches, one ball-cam amplifier, and an electromagnetic applying system to generate the compression force of the primary clutch, the detailed modeling method can be found in [17]. In this paper, the system is simulated by adding a first-order delay system with the time constant setting to be 25ms, which means it will take 100ms to reach 98% of the commanded torque output.

2) ACTIVE FRONT STEERING (AFS)

The control system flow diagram is shown in Fig. 5. The AFS controller acts as an additional and auxiliary tool to make amendment to the steering behavior of the driver based on the current vehicle states. The control algorithm for the individual AFS system is as shown in equation (9),

$$\delta_{AFS} = \frac{1}{1 + \tau_{AFS}s} \cdot \frac{\Delta M_c}{t_w \cdot \cos(\delta_{driver}) \cdot C_f} \tag{9}$$

where ΔM_c is the control yaw moment derived from the AFS actuator, the calculation of which is based on sliding mode control of the yaw rate, the details can be seen in [7], and C_f is the front tire cornering stiffness. The AFS actuator is deemed as a first-order delay system with the time constant τ_{AFS} set to 20ms. The amplitude and rate constraints of AFS actuator will be addressed in detail in the control allocation section.

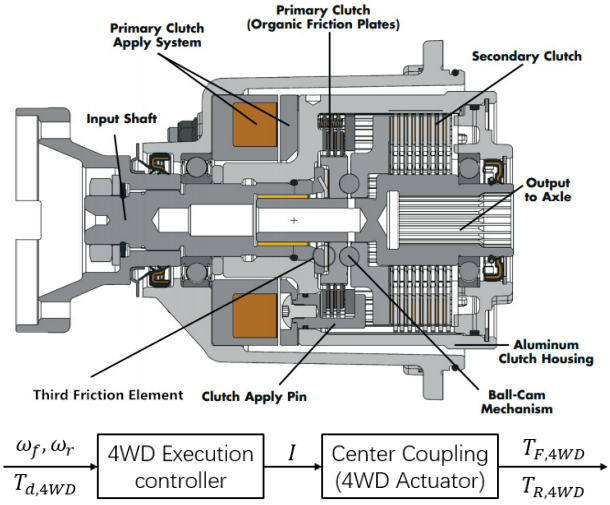

FIGURE 4. The profile structure and control flow of 4WD center coupling.

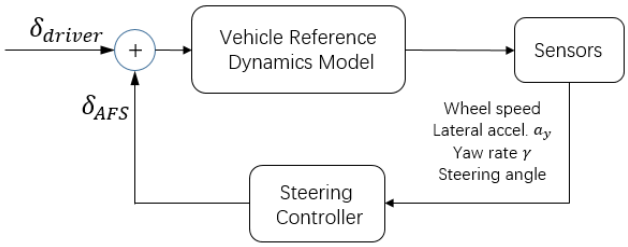

FIGURE 5. Diagram of AFS control system.

3) ELECTRONIC STABILITY CONTROL (ESC)

The differential braking commands are generated by the yaw moment controller considering the yaw motion error, the geometric relationship between the generated control yaw moment and the differential braking forces.

$$\begin{cases} m\dot{v}_x = (\overline{F_{xfl}} + \overline{F_{xfr}})\cos\delta_f - (\overline{F_{yfl}} + \overline{F_{yfr}})\sin\delta_f + (\overline{F_{xrl}} + \overline{F_{xrr}}) + mv_y\gamma \\ m\dot{v}_y = (\overline{F_{yfl}} + \overline{F_{yfr}})\cos\delta_f + (\overline{F_{xfl}} + \overline{F_{xfr}})\sin\delta_f + (F_{yrl} + F_{yrr}) - mv_x\gamma \\ I_z \cdot \dot{\gamma} = [(\overline{F_{yfl}} - \overline{F_{yfr}})\sin\delta_f - (\overline{F_{xfl}} - \overline{F_{xfr}})\cos\delta_f]t_w/2 - (F_{yrl} + F_{yrr})l_r - (\overline{F_{xrl}} - \overline{F_{xrr}})t_w/2 \\ \overline{F_{xii}} = F_{xii,4WD} - F_{xii,ESC}, \quad ii = fl, fr, rl, rr \overline{F_{yii}} = F_{yii} - \Delta F_{yii} \end{cases} \tag{1}$$

Usually the lateral motion of vehicle is controlled by hierarchical layers, then virtual control input of the upper-level controller ΔM_B can be achieved by the control of yaw rate or vehicle side slip. Similarly, the ESC system can be treated as a first-order delay system, the maximum braking pressure and the time constant, based on test data, are set to be 20bar and 30ms, respectively.

4) SIMULATION VERIFICATION OF INDIVIDUAL CONTROL SYSTEM

To implement the control algorithms, some of the vehicle states are essential to be estimated [18]–[21]. The estimator utilized in this paper is responsible for estimating the longitudinal velocity, vehicle sideslip angle and tire cornering stiffness based on the measured vehicle states by the pre-equipped sensors. Vehicles mounted with ESC system already are equipped with sensors like the four wheel speed sensors, steering wheel angle sensor, longitudinal/lateral acceleration sensor and yaw rate sensor. Then on the basis of these easily measured state signals, the hard-to-measure states can be estimated. Using the non-slip or minor-slip wheel speed in accelerating or decelerating condition and integrating a low-pass filter, the longitudinal velocity can be estimated [22]. Then the vehicle and tire sideslip angle can be estimated utilizing the longitudinal velocity, lateral acceleration, front wheel steering angle and the yaw rate with the method detailed in [23], [24]. The cornering stiffness in this paper, is estimated by simply using the off-line Magic Formula tire model based on the estimation of tire sideslip angles.

The overall estimator used in this paper is illustrated in Fig. 6.

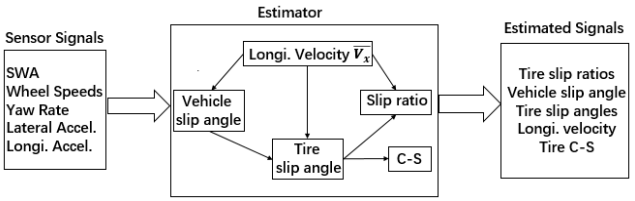

FIGURE 6. Diagram of the state estimator.

The performance of the individual control system of the chassis modules is verified using the co-simulation of Carsim and Matlab/Simulink, in which a closed-loop driver model in Carsim is used [25] and the actuator models have been validated through the test data of the real vehicle. In order to evaluate the effectiveness of AFS, the driver model's preview time is set to be 0.75s, which indicates an inexperienced driver. The simulations are conducted on circular turning (R=50m) and hairpin test road (R=30m) to evaluate the control performance in terms of understeer gradient (SWA/Ay), and individual lap time of the control algorithms. All the simulations are to test the limit performance without losing stability for the vehicle. When testing one specific control algorithm, the vehicle model is set to have only one control module, i.e. the vehicle is only mounted with front wheel driving and ordinary ABS when test AFS, and likewise for the other two modules. The simulation conditions are listed in Table 1 as follows.

TABLE 1. Simulation scenarios.

SCENARIO	VELOCITY (KPH)	SWA
HAIRPIN	MAXIMUM	DRIVER MODEL
CIRCULAR TURNING	60-150	DRIVER MODEL

TABLE 2. Simulation results of the individual control module.

ROAD CONDITION	INDICATOR	AFS	ESC	4WD
CIRCULAR TURNING	SWA/AY	-17%	-60%	-34%
HAIRPIN	LAP TIME	-1.2%	-0.3%	-2.5%

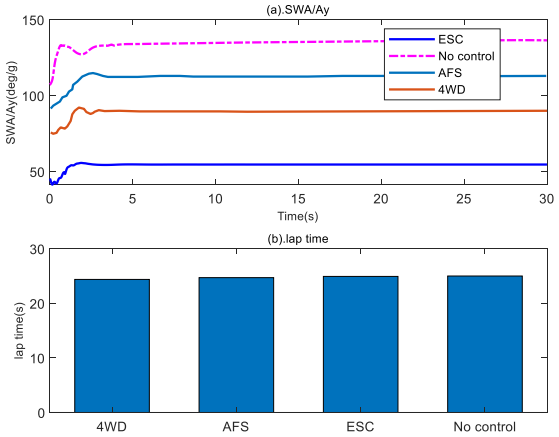

FIGURE 7. Simulation results of the individual system.

The control effects of the three modules compared with the 'no control' system regarding the maximum lateral acceleration and lap time are illustrated in Fig. 7. In comparison with the only ABS mounted vehicle, the statistical presentation is shown in Table 2. As shown in Table 2, 4WD can decrease the lap time by 2.5% corresponding to the 34% decreased understeer gradient, while the ESC can only shorten the lap time by 0.3% even though it can significantly decrease the understeer gradient by 60%, simply due to the fact that ESC functions based on deceleration of the tires. AFS can assist the driver to reach to the limit handling of the front tire, which helps maintain lateral stability confined by the friction condition of the front tires, thus the effect of AFS on reducing lap time is moderate compared with the other two control modules. It can be concluded from the above analysis that, 4WD is mainly dedicated to increasing vehicle speed and reducing lap time, while AFS and ESC contribute to maintaining stable lateral motion. Theoretically, together, the three systems can enhance the limit cornering performance of the vehicle if tuned properly.

III. COORDINATED CONTROL ALGORITHM

To make full use of the control degrees of freedom brought about by the various chassis modules rather than simple combination of the different control algorithms, a coordinated chassis control algorithm combined with control allocation optimal distribution need to be devised. Usually, a normal front-wheel-drive vehicle without control modules like AFS

or ESC is inclined to have uneven tire force distribution, the tires on the front axle tend to reach to a saturated state earlier. Based on the nonlinear coupling of longitudinal and lateral tire forces, the lateral force modification of AFS, and the driving/braking torque distribution brought about by 4WD and ESC can help release the saturated tires and optimally make the four tires saturated simultaneously with the assist of the coordinated control algorithm.

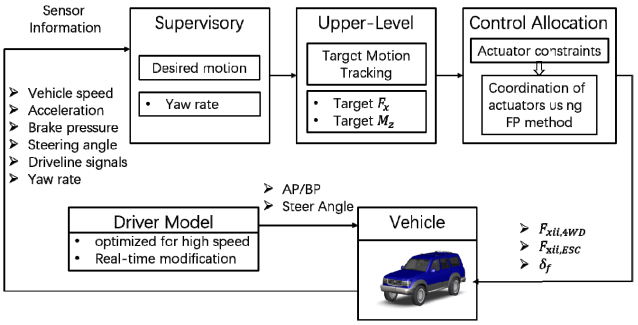

FIGURE 8. Architecture of the coordinated control algorithm AP/BP: acceleration pedal/braking pedal signals.

The proposed algorithm in this paper, as shown in Fig. 8, consists of three layers: the supervisory layer, the upper layer, and the control allocation layer. The supervisory controller is responsible for determining the desired yaw rate considering the steering wheel input, the vehicle speed and the vehicle dynamics limitations. The upper-level controller is designed to track the desired vehicle motion by calculating the target yaw moment and longitudinal forces. The control allocation layer utilizes the optimal control method, Fixed-Point (FP) method, to distribute the optimal actuator commands, i.e. the input current for 4WD, the brake pressure for ESC and the steering angle modification for AFS.

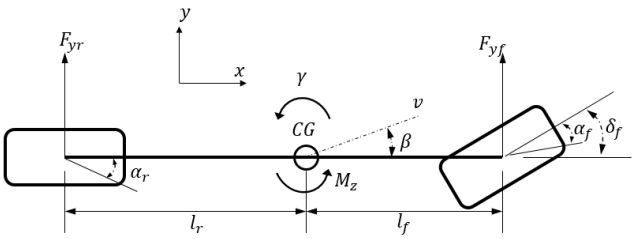

FIGURE 9. Schematic figure of 2 DOF vehicle model.

A. SUPERVISORY CONTROLLER DESIGN

The 2 DOF vehicle dynamics model including a control yaw moment is shown in Fig. 9, the corresponding vehicle dynamics can be expressed as,

$$\begin{bmatrix} \dot{\beta} \\ \dot{\gamma} \end{bmatrix} = \begin{bmatrix} -\frac{C_{\alpha f}+C_{\alpha r}}{mv_x} & \frac{l_r C_{\alpha r}-l_f C_{\alpha f}}{mv_x^2}-1 \\ \frac{l_r C_{\alpha r}-l_f C_{\alpha f}}{I_z} & -\frac{l_r^2 C_{\alpha r}+l_f^2 C_{\alpha f}}{I_z v_x} \end{bmatrix} \begin{bmatrix} \beta \\ \gamma \end{bmatrix} + \begin{bmatrix} \frac{C_{\alpha f}}{mv_x} \\ \frac{l_f C_{\alpha f}}{I_z} \end{bmatrix} \delta_f + \begin{bmatrix} 0 \\ \frac{1}{I_z} \end{bmatrix} M_z \tag{10}$$

$$a_y = v_x(\dot{\beta}+\gamma) \tag{11}$$

From the steady state relationship of steering wheel angle and the lateral acceleration, the desired yaw rate considering the transient cornering dynamics can be obtained by solving the equation (12) as follows [13],

$$\dot{\gamma}_{des} = -\frac{lC_{\alpha f}C_{\alpha r}}{I_z(C_{\alpha f}+C_{\alpha r})} \cdot \left[\frac{l}{v_x} + \left(\frac{ml_r}{C_{\alpha f}l} - \frac{ml_f}{C_{\alpha r}l}\right) \cdot v_x\right] \cdot \gamma_{des} + \frac{lC_{\alpha f}C_{\alpha f}}{I_z(C_{\alpha f}+C_{\alpha r})} \cdot \delta_f \tag{12}$$

The desired yaw rate will be resolved every time step, and the target yaw rate can be obtained by considering the vehicle-road dynamics limitation as,

$$\gamma_{target} = \min\left(\frac{\gamma_{des}}{1+\tau_e s}, 0.85 \cdot \frac{\mu g}{v_x}\right) \tag{13}$$

where τ_e is a time constant.

B. UPPER-LEVEL CONTROLLER

The target longitudinal force and yaw moment are determined in the upper level controller to track the desired motions. In consideration of the uncertainties in the dynamics modeling and external disturbances, the sliding mode control theory based on previous researches is applied here [26]–[28].

1) TARGET LONGITUDINAL FORCE

As for the target longitudinal motion dynamics, the desired longitudinal deceleration can be achieved utilizing the master cylinder pressure collected from sensors and the desired acceleration can be calculated with the information of the transmission system such as the engine output torque, gear ratios and transmission efficiency.

Then the desired longitudinal forces based on the driver input can be calculated by multiplying the gear ratios or the brake gains to the desired longitudinal acceleration or deceleration, respectively.

However, in steering scenario, the lateral stability of the vehicle, which is closely related to longitudinal speed, should be considered. The desired speed can be obtained based on the relationship of longitudinal velocity and the desired curvature by considering the physical limit of steering angle, tire-road friction and rollover prevention. The admissible control region was proposed to decide the velocity limit on the specified path in [29]. The target velocity in the next instant of time can be calculated as follows,

$$v_{target} = f(\kappa) = \begin{cases} \sqrt{\frac{\delta_f}{\kappa \cdot A_{steer}} - \frac{l}{A_{steer}}}, & \text{if } (v_x \le v_{eq}) \\ \sqrt{\frac{\min(0.85 \cdot \mu g,\ 0.9a_{y,\max})}{\kappa}}, & \text{if } (v_x > v_{eq}) \end{cases} \tag{14}$$

$$A_{steer} = \frac{m \cdot l_r}{2 \cdot C_{\alpha f} \cdot l \cdot \cos\delta_f} - \frac{m \cdot l_f}{2 \cdot C_{\alpha r} \cdot l} \tag{15}$$

where, κ is the curvature of the pre-specified path, A_{steer} is the understeer gradient, and v_{eq} denotes the solution of the

following equation:

$$\frac{\delta_f}{A_{steer} \cdot v_{eq}^2 + l} = \frac{\min(0.85 \cdot \mu g, 0.9 a_{y,\max})}{v_{eq}^2} \tag{16}$$

where $a_{y,\max}$ is the maximum lateral acceleration for vehicle lateral stability and rollover prevention, the calculation of which is detailed in [29].

To obtain the target longitudinal force based on the target longitudinal velocity as a virtual input in the supervisory controller, and to avoid the effect of external disturbances [30] on the control system, the sliding surface and the sliding condition can be defined as follows,

$$s_{vx} = v_x - v_{target}, \quad \frac{1}{2}\frac{d}{dt}s_{vx}^2 = s_{vx}\dot{s}_{vx} \le -\eta\,|s_{vx}| \tag{17}$$

where, η is a positive constant. To get the term $\dot{s}_{vx}$, we can assume small steering angle and rewrite the vehicle dynamics Equation (1) as follows,

$$\dot{v}_x = \frac{1}{m}(F_{xf} - F_{yf}\sin\delta_f + F_{xr}) + v_y\gamma - \frac{1}{m}F_{target} \tag{18}$$

Then the target longitudinal force achieved from the sliding condition is presented by equation (19).

$$F_{target} = (ma_x - C_{\alpha f}\alpha_f \sin\delta_f) + m(v_y\gamma - \dot{v}_{target}) - \xi_{vx} \cdot \mathrm{sat}(\frac{v_x - v_{target}}{\Phi_{vx}}) \tag{19}$$

The saturation function is used here to eliminate the chattering of the high-frequency control input, and the saturation function is defined as follows,

$$\mathrm{sat}(\frac{v_x - v_{target}}{\Phi_{vx}}) = \begin{cases} \mathrm{sgn}(v_x - v_{target}), & \left|\frac{v_x - v_{target}}{\Phi_{vx}}\right| > 1 \\ \left|\frac{v_x - v_{target}}{\Phi_{vx}}\right|, & \left|\frac{v_x - v_{target}}{\Phi_{vx}}\right| \le 1 \end{cases} \tag{20}$$

In equation (19), ξ_{vx} is a constant that satisfies the sliding condition of equation (17), it can be obtained as follows,

$$\xi_{vx} \le -\eta \cdot m \tag{21}$$

The determination of target longitudinal force based on the target velocity can be found in detail in [31].

2) TARGET YAW MOMENT

The two major tasks of the vehicle stability control are minimizing the yaw rate tracking error and maintaining small vehicle side-slip angle. Thus, to put more emphasis on the stability in steering, the desired vehicle side slip angle in neutral steering can be set as $\beta_{des} = 0$, then utilizing sliding mode control algorithm, the slide surface and sliding condition can be designed as,

$$s_{yaw} = \gamma - \gamma_{des} + \xi_{Mz}\beta, \quad \dot{s}_{yaw} = -\lambda s_{yaw}(\lambda > 0) \tag{22}$$

Then by integrating equations (10) and (11), and eliminating the vehicle side slip, the following equation can be obtained.

$$\dot{\gamma} = -\frac{2C_{\alpha f}C_{\alpha r}}{C_{\alpha f} + C_{\alpha r}} \cdot \frac{(l_f + l_r)^2}{I_z v_x} \cdot \gamma + \frac{m(l_f C_{\alpha f} - C_{\alpha r} l_r)}{(C_{\alpha f} + C_{\alpha r})I_z} a_y + \frac{2C_{\alpha f}C_{\alpha r}}{C_{\alpha f} + C_{\alpha r}} \cdot \frac{(l_f + l_r)}{I_z}\delta_f + \frac{1}{I_z}M_z \tag{23}$$

The control yaw moment of the upper-level controller can then be obtained by satisfying the sliding condition (22),

$$M_z = \left(\frac{2C_{\alpha f}C_{\alpha r}}{C_{\alpha f} + C_{\alpha r}} \cdot \frac{(l_f + l_r)^2}{v_x} - I_z\lambda\right) \cdot \gamma - \frac{2C_{\alpha f}C_{\alpha r}(l_f + l_r)}{C_{\alpha f} + C_{\alpha r}}\delta_f - \left(\frac{m(l_f C_{\alpha f} - C_{\alpha r} l_r)}{C_{\alpha f} + C_{\alpha r}} + \frac{I_z\lambda}{v_x}\right) \cdot a_y + I_z \cdot \dot{\gamma}_{target} - K_\gamma \cdot \mathrm{sat}(\frac{S_{yaw}}{\Phi_{yaw}}) \tag{24}$$

C. CONTROL ALLOCATION LAYER

For an over-actuated vehicle, the control allocation is essential as regard to optimally allocating the controlled longitudinal tire forces and the target yaw moment to the actuators. The optimal control allocation algorithm is designed based on an optimization control method considering such factors as the actuators limits and the vehicle-road friction limits. The goal and constraints of control allocation algorithm can be summarized into four parts: 1. minimizing the allocation error when mapping the virtual controls of upper-level controller inputs to the real actuator input commands; 2. minimizing the overall slips of the four wheels, both longitudinal and lateral; 3. minimizing the unwilling braking by ESC; 4. considering the actuator limits and the vehicle-road friction limits.

1) MINIMIZATION OF UNWILLING BRAKING BY ESC

Braking during the normal driving can cause unpleasant driving experience and even unnecessary wear and tear. Then the cost function of the unwilling braking by ESC can be expressed as:

$$J_1 = \|W_{u1}u(t)\|^2 \tag{25}$$

where, W_{u1} is the diagonal weighting matrix of the actuator inputs.

2) MINIMIZATION OF OVERALL SLIPS OF THE TIRES

In condition of limit handling, the tire-road friction usage of the tires differs largely from each other. To fully utilize the vehicle-road friction limits, a number of previous researches [31], [32] have been centered on the even distribution of tire forces to make the friction utilization similar to each other. However, due to the difficulty-to-measure feature and the nonlinearity of tire forces, the method of monitoring the tire workload used in those researches can be unsuitable for implementation in practical scenario. Then the tire slip

TABLE 3. The parameters in penalty function.

PARAMETERS	VALUES
a_{hyper}	9
$\hat{\eta}_{peak,i}$	0.1
b_{hyper}	3

penalty function method proposed in [13] is adopted in this paper.

First, define the combined slip of an individual tire as:

$$\begin{cases} \eta_i = \sqrt{\eta_{xi}^2 + \eta_{yi}^2}, & i = fl, fr, rl, rr \\ \eta_{xi} = \dfrac{s_{xi}}{1 + s_{xi}}, & \eta_{yi} = \dfrac{\alpha_i}{1 + \alpha_i} \end{cases} \tag{26}$$

where η_i is the combined slip of each wheel; η_{xi}, η_{yi} are the modified slip ration and slip angle of each tire, respectively; and s_{xi}, α_i are the slip ratio and slip angle of each wheel, respectively.

Then, the overall slip-based penalty of each tire usage can be defined as follows, (27), as shown at the bottom of this page, where, $\eta_{peak,i}$ is the peak combined slip of the tire; a_{hyper}, b_{hyper} are the tuning parameters of the penalty function; $\bar{\mu}$ is the road friction coefficient, which can be estimated with the assist of GPS measurements and an accelerometer [33]. The values of the parameters in the equation are set as in Table 3.

Then the variation of the hyperbolic penalty against the individual tire combined slip, and the two asymptotes of the hyperbolic penalty, as shown in equation (28), are illustrated in Fig. 10.

$$y = 2a_{hyper}(\eta_i - 0.5 \cdot \eta_{peak,i})/\eta_{peak,i} y = 0 \tag{28}$$

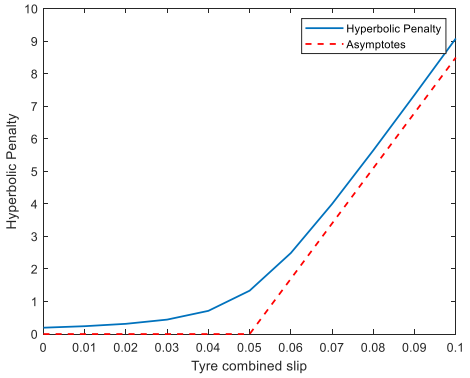

$F_z = 4000, \mu = 0.8.$

FIGURE 10. Hyperbolic penalty: $F_z = 4000, \mu = 0.8$.

The monotonically increasing feature of the hyperbolic penalty function makes it applicable to formulate a tire saturation cost function by multiplying the longitudinal tire force to the corresponding penalty. Then the controller can allocate the excessive longitudinal force to the less saturated tires to keep the friction usage similar for the four tires, thus, the tire-road friction can be fully utilized and the vehicle limit handling performance can be improved. The cost function of tire usage is defined as:

$$\begin{bmatrix} p_{fl} & 0 & 0 & 0 \\ 0 & p_{fl} & 0 & 0 \\ 0 & 0 & p_{fl} & 0 \\ 0 & 0 & 0 & p_{fl} \end{bmatrix} \cdot \underbrace{B_{longi\_force} \cdot u(t)}_{[F_{xfl}, F_{xfr}, F_{xrl}, F_{xrr}]^T} = \underbrace{B_2}_{[4\times8]} \cdot \underbrace{u(t)}_{[8\times1]} \tag{29}$$

$$J_2 = \|W_{v2}(B_2 \cdot u(t))\|^2 \tag{30}$$

where, B_{longi_force} is the longitudinal force expression matrix; B_2 is the tire saturation penalty matrix, and W_{v2} is the diagonal weighting matrix.

3) MINIMIZATION OF THE ALLOCATION ERROR

The target yaw moment and the longitudinal force have been determined in the previous sections. The theoretical relationship between the actual control inputs and the virtual control commands can be described as follows,

$$\begin{aligned} &F_{x,target} \\ &= \underbrace{F_{xf,4WD} + F_{xrl,4WD} + F_{xrr,4WD}}_{F_{x,4WD}(\text{acceleration pedal})} \\ &\quad - \underbrace{(F_{x,fl,ESC} + F_{x,rl,ESC} + F_{x,rl,ESC} + F_{x,rr,ESC})}_{F_{x,ESC}(\text{brake pedal})} \end{aligned} \tag{31}$$

$$\begin{aligned} &M_{z,target} \\ &= \underbrace{(-F_{x.rl,4WD} + F_{x.rr,4WD}) \cdot l_f}_{\text{indirect yaw moment}} + \underbrace{C_{\alpha f} \cdot l_f \cdot \Delta\delta_f}_{\text{AFS}} \\ &\quad + \underbrace{\frac{t_w}{2} \cdot (F_{x,fl,ESC} - F_{x,fr,ESC} + F_{x.rl,ESC} - F_{x.rr,ESC})}_{\text{direct yaw moment}} \end{aligned} \tag{32}$$

$$\begin{aligned} &u(t) \\ &= [F_{xf,4WD}, F_{xrl,4WD}, F_{xrr,4WD}, F_{x,fl,ESC}, \\ &\quad F_{x,rl,ESC}, F_{x,rl,ESC}, F_{x,rr,ESC}, \delta_f]^{\mathrm{T}} \end{aligned} \tag{33}$$

$$P_i = 0.1 \cdot \bar{\mu}\hat{F}_z / \left(\begin{array}{l} -a_{hyper} \cdot \dfrac{(|\hat{\eta}_i| - 0.5 \cdot \hat{\eta}_{peak,i})}{\hat{\eta}_{peak,i}} \\ + \sqrt{\left\{ a_{hyper} \cdot \dfrac{(|\hat{\eta}_i| - 0.5 \cdot \hat{\eta}_{peak,i})}{\hat{\eta}_{peak,i}} \right\}^2 + b_{hyper}^2} \end{array} \right) \tag{27}$$

where, $u(t)$ is the actuator control input. The matrix form of the three equations above can be written as,

$$\underbrace{\begin{bmatrix} F_{x,acc.} \\ F_{x,dec.} \\ M_{z,target} \end{bmatrix}}_{v_3(t)[3\times 1]} = \underbrace{\begin{bmatrix} 1 & 1 & 1 & 0 & 0 & 0 & 0 & 0 \\ 0 & 0 & 0 & -1 & -1 & -1 & -1 & 0 \\ 0 & -l_f & l_f & 0.5t_w & -0.5t_w & 0.5t_w & -0.5t_w & C_{\alpha f}\cdot l_f \end{bmatrix}}_{B_3[3\times 8]} \cdot u(t) \tag{34}$$

where, $v_1(t)$ is the virtual control input vector and B_1 is the control effectiveness matrix, also known as the allocation matrix. The signs of the elements are determined in accordance to the settings in Carsim. Then the cost function for minimizing the control allocation error can be defined as:

$$J_3 = \|W_{v3}(B_3 u(t) - v_3(t))\|^2 \tag{35}$$

where W_{v3} is the diagonal weighting matrix.

4) ACTUATOR CONTROL LIMIT CONSTRAINTS

There are constraints on the actuators controlling, such as the actuators physical limit and rate limit, and the controlling limit in the limit handling scenario for the vehicle. Note that the controlling of each actuator is closely related to the vehicle dynamics, then at the given instant of time, the actuators functioning range can be limited by the real-time vehicle dynamics.

The mechanical mechanism of the 4WD actuator presented in this paper is, as shown in Fig. 4, a central multi-plate coupling controlled by an electromagnetic device and an electronically controlled slip-limited clutch. Unlike the layout of in-wheel motors, vehicle presented in this paper has limited driving torque distribution ratios. According to the technical analysis of the prototype car used in this research, the maximum rear/front torque distribution ratio is 0.61 and the maximum rear left/rear right torque distribution ratio is 0.5, which means the maximum torque transferred to the rear axle is $0.61 \cdot T_{trans}$, and the maximum torque transferred to the one side on the rear axle is $0.5 \cdot T_{rear}$. In addition, the longitudinal tire force is confined by the vertical tire force, as follows,

$$F_{xii,\max} = \sqrt{(\mu F_{zii})^2 - F_{yii}^2} \tag{36}$$

where, $F_{xii,\max}$ is the limit of individual longitudinal tire force. Then due to the difficulty of measuring lateral tire forces in practice, the latter part of equation (36) is removed. With the tire saturation penalty aforementioned above, this over-estimated upper limit of longitudinal force will be effectively avoided. Then the 4WD actuator limit constraints can be described as:

$$\begin{cases} 0 \le F_{xf,4WD} \le \min(\sqrt{(\mu F_{zf})^2}, T_{trans}/r) \\ 0 < F_{xi,4WD} \le \min(0.5 \cdot 0.61 \cdot T_{trans}/r, \sqrt{(\mu F_{zi})^2}), \\ \qquad\qquad i = rl, rr \end{cases} \tag{37}$$

where, r is the effective radius of the wheel, $F_{xf,4WD}$ is the 4WD driving force acting on the front wheels, and F_{zf} denotes the vertical force on the front wheels.

The exertion of auxiliary front steering by AFS has to comply with the physical limit of front wheel steering and the requirement of the vehicle stability of lateral dynamics. The upper limit of the front wheel steering angle can be calculated with given vehicle information of last instant of time as follows,

$$\delta_{f,\max} = \alpha_{f,\max} + \frac{\dot{y}(t) + l_f \dot{\gamma}(t)}{v_x(t)} \tag{38}$$

where, $\alpha_{f,\max}$ is the maximum allowed stable tire slip angle, and $y(t)$ is the lateral position of the vehicle. The maximum tire slip angle can be obtained by solving the partial differential equation of $\partial F_{yi}/\partial \alpha_i = 0$ based on the Magic Formula tire model, which is quite complicated that it requires tons of computation time and takes up too much computation resource. Note that the tire slip angle limit only changes against the tire-road friction coefficient and is not related to other vehicle state parameters [34]. Then a sufficiently accurate approximate method for obtaining $\alpha_{f,\max}$ can be illustrated by the shaded area, as the effective regions of operation, in Fig. 11.

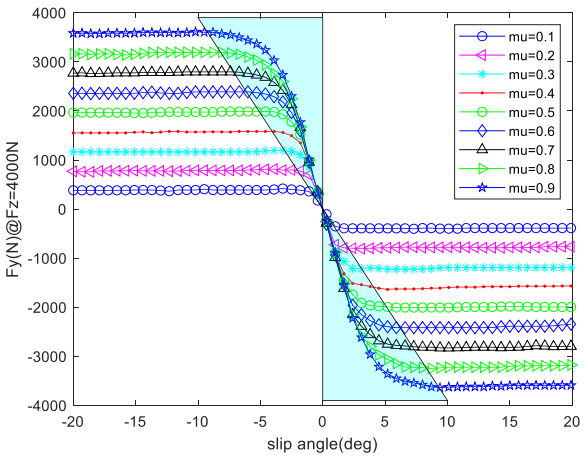

FIGURE 11. Relation of tire lateral force and slip angle with variation of friction coefficient.

The maximum slip angle against different friction can then be obtained by interpolation with a 2D look-up table obtained from Fig. 11.

In the limit handling scenario, $\dot{y}(t)$ can be negligible assuming small side-slip angle of the vehicle. Then the AFS actuator limit constraints is described as:

$$0 \le |\delta_f| \le \min\left(\delta_{\max}, \alpha_{f,\max} + \frac{l_f \dot{\gamma}(t)}{v_x(t)}\right) \tag{39}$$

where, $\delta_{\max}$ is the physical limit of the front wheel steering angle.

The brake actuator limit is mainly due to the limit of the compression force the ESC actuator can exert. Then the constraint of ESC can be expressed as:

$$0 \le F_{xii,ESC} \le p_{\max} \cdot \phi_{ESC}, \quad ii = fl, fr, rl, rr \tag{40}$$

where, ϕ_{ESC} is the gain between the braking pressure and the actual braking force.

With the above analyses, the overall limit constraints of all the actuators can be summarized as:

$$\begin{cases} u_{\min} = [0, 0, 0, 0, 0, 0, 0, 0]^{\mathrm{T}} \\ u_{\max} \\ = \begin{bmatrix} F_{f,4WD,\max}, F_{rl,4WD,\max}, F_{rr,4WD,\max}, F_{fl,ESC,\max}, \\ F_{fr,ESC,\max}, F_{rl,ESC,\max}, F_{rr,ESC,\max}, \delta_{f,\max} \end{bmatrix}^{\mathrm{T}} \end{cases} \tag{41}$$

The terms in the expression of $u_{\max}$ are the upper limits of the 4WD driving force in the front axle/rear-left wheel/rear-right wheel, ESC braking force in the front-left/front-right/rear-left/rear-right wheel, and the road wheel steer angle by AFS, respectively.

5) OPTIMAL DISTRIBUTION OF THE CONTROLS

With the analyses provided above, the optimal distribution of the controls can be expressed as a weighted least-squares (WLS) problem, as shown in equation (42).

This WLS problem can be solved by the fixed-point algorithm [35]. Then the distributed control will be the optimal control inputs for AFS, 4WD and ESC. Then, the actual actuator inputs, i.e., the control current of 4WD and the brake pressure of the ESC can be calculated.

$$\begin{aligned} & u(t) \\ & = \arg\min_{U \le u \le \bar{U}} [\xi_{u1} \cdot J_1 + \xi_{v2} \cdot J_2 + \xi_{v3} \cdot J_3] \\ & = \arg\min_{U \le u \le \bar{U}} \left\{ \left\| \underbrace{\begin{pmatrix} \xi_{v2}^{1/2} \cdot W_{v2} \cdot B_2 \\ \xi_{v3}^{1/2} \cdot W_{v3} \cdot B_3 \\ \xi_{u1}^{1/2} \cdot W_{u1} \end{pmatrix}}_{A} u - \underbrace{\begin{pmatrix} 0 \\ \xi_{v3}^{1/2} \cdot W_{v3} \cdot v_3 \\ 0 \end{pmatrix}}_{b} \right\|^2 \right\} \\ & = \arg\min_{U \le u \le \bar{U}} (\|A \cdot u - b\|^2) \end{aligned} \tag{42}$$

IV. SIMULATION AND COMPARISON

To evaluate the performance of the designed algorithm regarding the yaw moment distribution and tire usage, two simulation tests utilizing Matlab/Simulink and Carsim are carried out. The first test scenario is a double lane change conducted at a given throttle opening acceleration and a given braking M/C pressure deceleration respectively with a closed-loop driver-vehicle-controller system. This scenario is comparatively common in accelerating to overtake other cars or in avoiding collision occasion. The second scenario is a simulation on a handling course to verify the comprehensive performance of the proposed algorithm.

TABLE 4. Main parameters of the prototype car.

TYPE	UNIT	VALUE
m	kg	2162
l_f	mm	1104.3
l_r	mm	1595.7
I_z	$kg \cdot m^2$	3234.0
t_w	mm	1555
TIRE SIZE	---	225/65R17

The designed algorithm will be compared with three other control systems to validate the effectiveness and handling enhancement: (1) only anti-lock braking system (ABS) equipped system (marked as Base); (2) four-wheel independent brake controlled system (marked as 4IB); (3) an integrated chassis control system by means of front/rear traction control and four-wheel independent braking (marked as AWD-4IB) [13]. Vehicles equipped with the first three systems are both front wheel driven, just as the prototype vehicle. The proposed control system is different from the third system mainly in that, the AWD-4IB system doesn't include the active front steering control.

The vehicle model used in this simulation is a mid-size SUV with the parameters measured from a prototype vehicle, as shown in Table 4.

A. DOUBLE LANE CHANGE WITH ACCELERATION AND DECELERATION

In this section, the simulation of double lane change with acceleration and deceleration will be conducted. The initial speed is set to 75kph and 85kph in acceleration and deceleration respectively, and the tire-road friction coefficients of both scenario are set to 0.8. The driver model used in these simulations is obtained from Carsim and responsible for providing the steering input in a closed-loop steering maneuver. The preview interval of the driver is set to 0.75s.

The acceleration simulation is designed to model the normal driving scenario when the driver decides to change the lane. In the accelerating scenario, the acceleration action is exerted at 1s with the throttle opening spiking to 0.3, and the vehicle starts to steer at about 2s. The simulation results are shown in Fig. 12-13. As can be seen in Fig. 12, the four control algorithms have similar performance of tracking the route with regard to yaw rate, however, the uncontrolled vehicle (Base) shows some instability when returning to the straight line, in contrast, the other three control systems show better maneuverability.

To assess the usage of each tire, the TDEs of the four algorithms are calculated. The comparison of the TDE of the four systems is illustrated in Fig. 12(c). As can be seen in the figure, the TDE of the front wheels of both Base and 4IB systems are larger than that of the rear tires. On the contrary, the AWD-4IB and proposed control algorithm both

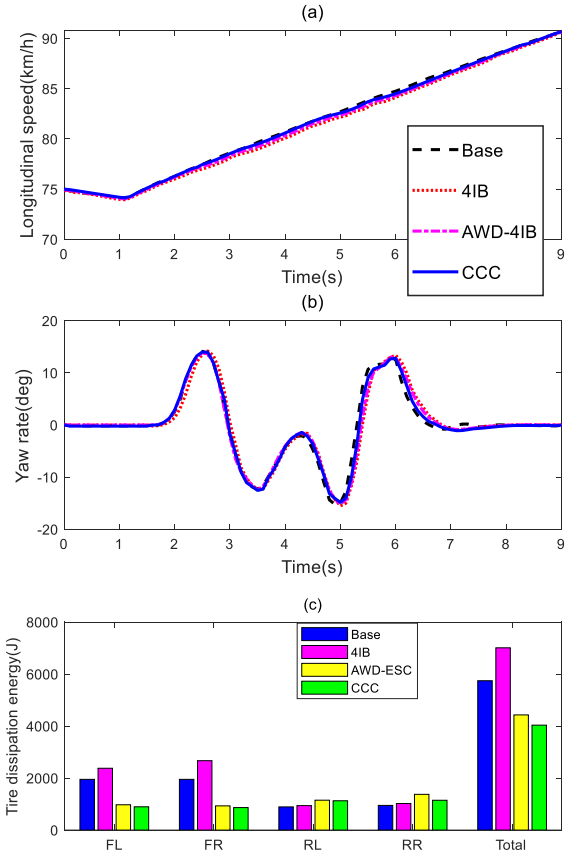

FIGURE 12. Double lane change with moderate acceleration.

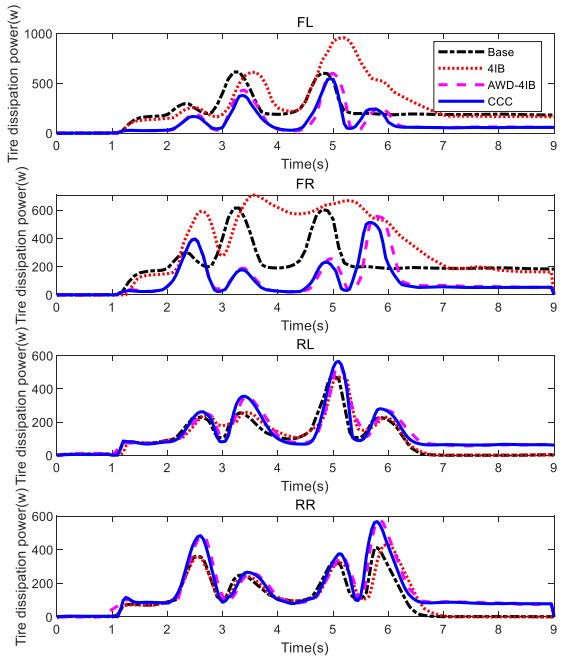

FIGURE 13. Tire dissipation power in double lane change with moderate acceleration.

maintain roughly even TDE for each wheel, this is because the latter two algorithms can allocate the traction forces. Meanwhile, they considerably reduce the total amount of the energy compared to that of Base and 4IB systems.

There are two points worth noting in Fig. 12: (1) TDE of 4IB system vehicle is larger than Base owing to the braking exertion in tracking the target yaw rate of the vehicle; (2) TDE of the AWD-4IB is slightly larger than that of the proposed algorithm because the proposed algorithm can adjust the steer wheel angle and redistribute the traction forces in the rear axles to better distribute the lateral and longitudinal tire forces to minimize the TDE, while the AWD-4IB equipped vehicle can only distribute the front/rear traction force and the four wheel braking forces.

The tire dissipation power (TDP) of each wheel is shown in Fig. 13, in which the legends FL,FR,RL and RR are symbols for the four wheels of the vehicle- front left, front right, rear left and rear right, respectively.. The TDP starts to increase at 1s when the throttle opening spikes to 0.3 and the traction forces start to be exerted to the driving wheels. It can be seen from Fig. 13 that, the tire usage of both AWD-4IB and CCC is evenly distributed due to the tire slip monitoring in the control algorithm, whereas, the front tire usage of Base and 4IB systems are obviously larger than that of the rear tires.

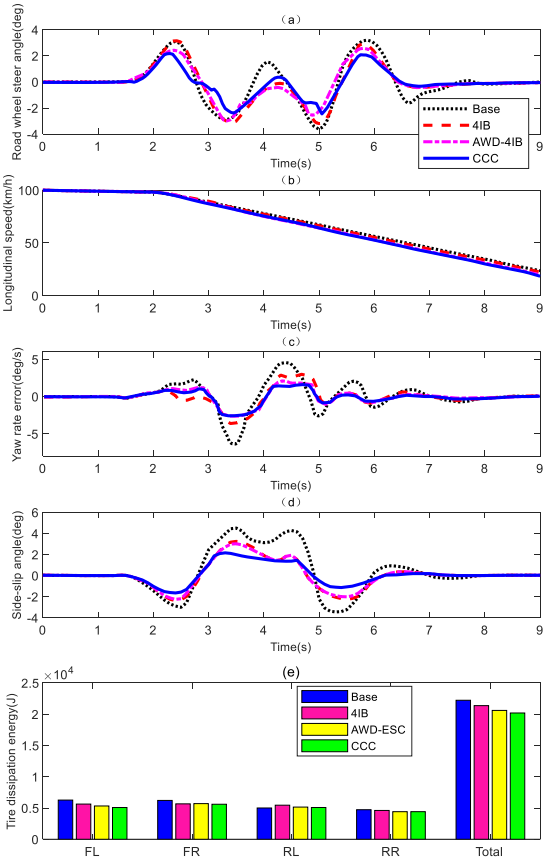

FIGURE 14. Aggressive double lane change with deceleration.

The simulation results of an aggressive double lane change with deceleration are shown in Fig. 14-15. It is assumed that the driver decides to brake the vehicle at 2s, with a force of 70N exerted on the brake pedal to produce an M/C pressure of about 2.56Mpa. The average longitudinal deceleration is 0.4g and the peak lateral acceleration is 0.6g.

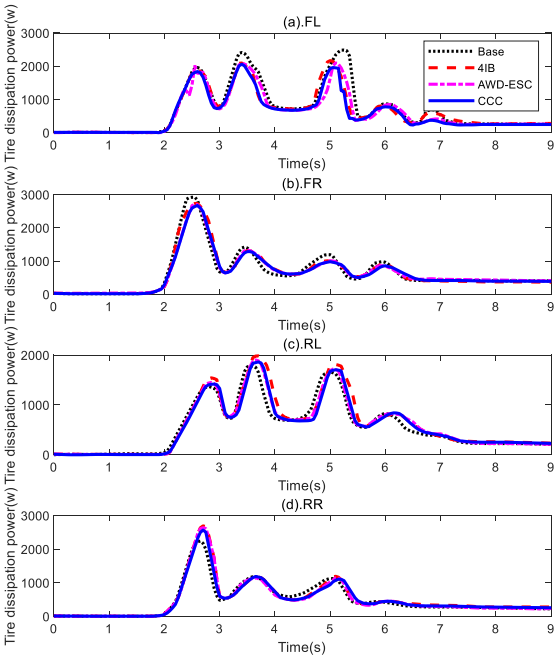

FIGURE 15. Tire dissipation power in double lane change with aggressive deceleration.

As can be seen in Fig. 14(a), the steering angle of proposed CCC can be considerably reduced during the aggressive cornering, which is realized with the coordination of AFS and four-wheel independent braking.

The handling performance of the four systems are illustrated in Fig. 14(c)-(d). The yaw rate error of the uncontrolled Base vehicle is relatively larger than that of the other three systems. Since the AWD-4IB system makes use of the four-wheel independent braking system during the deceleration just as the 4IB system, the difference of the handling performance of those two systems is minimal, as indicated by the index of vehicle side-slip angle illustrated in Fig. 14(d).

The TDE of each algorithm is shown in Fig. 14(e). The front wheel TDE of Base vehicle is slightly larger than that of the rear wheels because of the brake proportioning configuration. Whereas, the other three systems can distribute the braking torques of the four wheels to produce the desired yaw motion with minimization of the total tire usage. Thus, the total TDE of those three algorithms can be effectively reduced with comparison to that of the Base vehicle.

In conclusion, the proposed control system can effectively maintain the stability and enhance handling performance of the vehicle, meanwhile, it can significantly reduce the TDE both in moderate accelerating case and the aggressive braking during double lane change scenario.

B. COMPREHENSIVE TEST ON A HANDLING COURSE ROAD

To evaluate the comprehensive handling performance of the proposed algorithm, a simulation on an asphalt handling course road with Matlab/Simulink and Carsim is conducted. The segmented handling course road is shown in Fig. 16, the friction coefficient is se to 0.8. The simulation is performed on the entire road, but to evaluate the performance of the proposed algorithm in intensively, the detailed analysis is conducted on the segment 12-14.

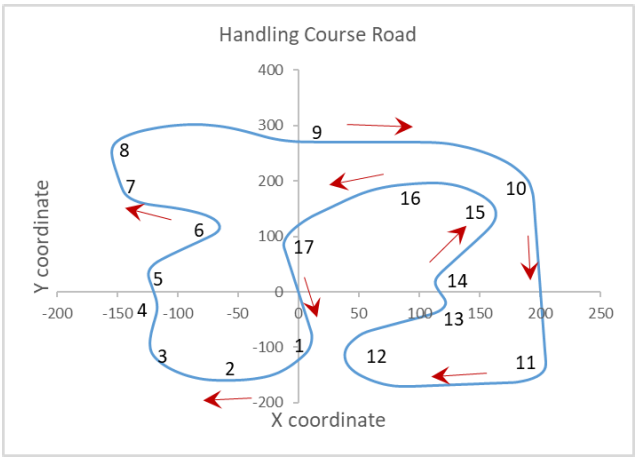

FIGURE 16. Handling course road by segments.

The driver model used in this simulation to generate the desired steering input and accelerating/decelerating input is obtained from previous research [36], in which the longitudinal and lateral parts are responsible for the throttle/brake and steering inputs, respectively.

The path-fitting algorithm [37], achieved with the reference of a skillful race driver's trajectory, is adopted to generate the reference path for the driver model to track. Upon obtaining the reference path, the reference velocity profile can be generated by applying with the fitted curvature profile [38].

With the reference velocity profile pre-calculated, the required input of steering wheel angle, throttle/brake inputs can be obtained from the driver model with the goal of tracking the reference velocity point by point.

Fig. 17 shows the simulation results of the comprehensive test on the handling road, the steering wheel angle, the longitudinal/lateral acceleration, the longitudinal velocity and the trajectory. The path tracking performance is similarly precise for the four algorithms, as illustrated in Fig. 17a. But as aforementioned before, Base and 4IB algorithms cannot monitor the tire usage conditions, hence, the total tire dissipation energy of them is larger than that of the other two algorithms, see Fig. 17b. With the coordination of AFS and AWD/4IB, the proposed algorithm manages to decrease the tire usage further compared with that of AWD-4IB algorithm, without compromising the handling performance of the vehicle. The longitudinal acceleration of CCC algorithm, as can be seen in Fig. 17d, is prominently larger than that of both of Base and 4IB algorithms, which is due to the better cornering performance and friction limit utilization of the proposed algorithm. The better utilization of tire-road friction enables the vehicle to decelerate later than those two algorithms when the vehicle enters the corner. As a result, the average longitudinal speed of the CCC is larger than that of those two algorithms, and

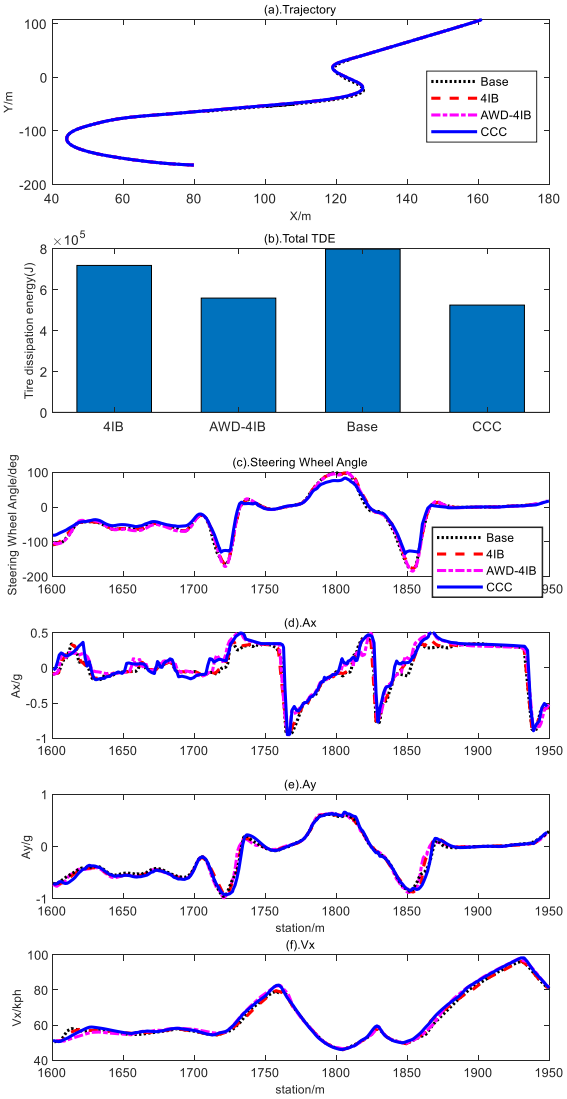

FIGURE 17. Simulation results of corner 12-14 on handling course road.

the lap time is reduced by 3.8% (4.3s) with comparison to the Base algorithm.

V. CONCLUSION

A coordinated control algorithm of the vehicle chassis utilizing differential braking, electronically controlled real-time 4WD and the active front steering is developed in this paper to obtain optimal coordination of the three individual control modules. A key point in this paper is the proposal of tire-slip penalty function, which makes the minimization of tire dissipation energy easier. On the basis of maintaining vehicle stability, the vehicle has more capability in limit handling with the less dissipation energy consumed in moderate driving.

The results of the double lane change simulations show that the proposed algorithm can enhance the limit handling performance in the aggressive driving scenarios and significantly reduce the overall tire usage in the meantime compared with Base, 4IB algorithms, and the ICC algorithm proposed in previous research.

The proposed chassis control algorithm can be applied for a constraint situation, and the performance of the system can be promoted with a higher-order sliding mode controller such as the second-order sliding mode controller. Given the excellent performance of the CCC in the simulations, real-car tests and real-time implementation to evaluate the performance of the proposed CCC algorithm are the topic of future work.

REFERENCES

[1] Q. Meng, C. Chen, P. Wang, Z. Sun, and B. Li, "Study on vehicle active suspension system control method based on homogeneous domination approach," *Asian J. Control*, pp. 1–11, Sep. 2019.

[2] Q. Meng, C. Qian, and R. Liu, "Dual-rate sampled-data stabilization for active suspension system of electric vehicle," *Int. J. Robust Nonlinear Control*, vol. 28, no. 5, pp. 1610–1623, 2016.

[3] B. A. Guvenc, T. Acarman, and L. Guvenc, "Coordination of steering and individual wheel braking actuated vehicle yaw stability control," in *Proc. IEEE IV Intell. Vehicles Symp.*, Columbus, OH, USA, 2003, pp. 288–293.

[4] S. Yim, S. Kim, and H. Yun, "Coordinated control with electronic stability control and active front steering using the optimum yaw moment distribution under a lateral force constraint on the active front steering," *Proc. Inst. Mech. Eng., D, J. Automobile Eng.*, vol. 230, no. 5, pp. 581–592, Apr. 2016.

[5] A. Goodarzi, A. Sabooteh, and E. Esmailzadeh, "Automatic path control based on integrated steering and external yaw-moment control," *Proc. Inst. Mech. Eng., K, J. Multi-Body Dyn.*, vol. 222, no. 2, pp. 189–200, Jun. 2008.

[6] S. J. Yim, "Unified chassis control with electronic stability control and active front steering for under-steer prevention," *Int. J. Automot. Technol.*, vol. 16, no. 5, pp. 775–782, Oct. 2015.

[7] S. Yim, "Coordinated control of ESC and AFS with adaptive algorithms," *Int. J. Automot. Technol.*, vol. 18, no. 2, pp. 271–277, Apr. 2017.

[8] M. Ataei, C. Tang, A. Khajepour, and S. Jeon, "Active camber system for lateral stability improvement of urban vehicles," *Proc. Inst. Mech. Eng., D, J. Automobile Eng.*, vol. 233, no. 14, pp. 3824–3838, Dec. 2019.

[9] A. Farazandeh, A. Ahmed, and S. Rakheja, "An independently controllable active steering system for maximizing the handling performance limits of road vehicles," *Proc. Inst. Mech. Eng., D, J. Automobile Eng.*, vol. 229, no. 10, pp. 1291–1309, Sep. 2015.

[10] Q. Meng, T. Zhao, C. Qian, Z.-Y. Sun, and P. Ge, "Integrated stability control of AFS and DYC for electric vehicle based on non-smooth control," *Int. J. Syst. Sci.*, vol. 49, no. 7, pp. 1518–1528, May 2018.

[11] C. March and T. Shim, "Integrated control of suspension and front steering to enhance vehicle handling," *Proc. Inst. Mech. Eng., D, J. Automobile Eng.*, vol. 221, no. 4, pp. 377–391, Apr. 2007.

[12] J. Guo, K. Li, and Y. Luo, "Coordinated control of autonomous four wheel drive electric vehicles for platooning and trajectory tracking using a hierarchical architecture," *J. Dyn. Syst., Meas., Control*, vol. 137, no. 10, Oct. 2015.

[13] E. Joa, K. Park, Y. Koh, K. Yi, and K. Kim, "A tyre slip-based integrated chassis control of front/rear traction distribution and four-wheel independent brake from moderate driving to limit handling," *Vehicle Syst. Dyn.*, vol. 56, no. 4, pp. 579–603, Apr. 2018.

[14] H. Her, Y. Koh, E. Joa, K. Yi, and K. Kim, "An integrated control of differential braking, Front/Rear traction, and active roll moment for limit handling performance," *IEEE Trans. Veh. Technol.*, vol. 65, no. 6, pp. 4288–4300, Jun. 2016.

[15] D. Piyabongkarn, J. Y. Lew, R. Rajamani, J. A. Grogg, and Q. Yuan, "On the use of torque-biasing systems for electronic stability control: Limitations and possibilities," *IEEE Trans. Control Syst. Technol.*, vol. 15, no. 3, pp. 581–589, May 2007.

[16] D. Piyabongkarn, J. Y. Lew, R. Rajamani, and J. A. Grogg, "Active driveline torque-management systems," *IEEE Control Syst. Mag.*, vol. 30, no. 4, pp. 86–102, Aug. 2010.

[17] A. Maroonian, T. Tamura, and R. Fuchs, "Modeling and simulation for the dynamic analysis of an electronically controlled torque coupling," *IFAC Proc. Volumes*, vol. 46, no. 21, pp. 464–469, 2013.

[18] J. Zhao, J. Zhang, and B. Zhu, "Coordinative traction control of vehicles based on identification of the tire-road friction coefficient," *Proc. Inst. Mech. Eng., D, J. Automobile Eng.*, vol. 230, no. 12, pp. 1585–1604, 2016.

[19] H. Xiao, W. Chen, H. Zhou, and J. W. Zu, "Integrated control of active suspension system and electronic stability programme using hierarchical control strategy: Theory and experiment," *Vehicle Syst. Dyn.*, vol. 49, nos. 1–2, pp. 381–397, Feb. 2011.
[20] S. Di Cairano and H. E. Tseng, "Driver-assist steering by active front steering and differential braking: Design, implementation and experimental evaluation of a switched model predictive control approach," in *Proc. 49th IEEE Conf. Decis. Control (CDC)*, Atlanta, GA, USA, Dec. 2010, pp. 2886–2891.
[21] X.-H. Chang and G.-H. Yang, "Nonfragile H_∞ filtering of continuous-time fuzzy systems," *IEEE Trans. Signal Process.*, vol. 59, no. 4, pp. 1528–1538, Apr. 2011.
[22] J. Oh and S. B. Choi, "Design of a new composite observer for vehicle velocity and attitude estimation," in *Proc. IASTED Int. Conf. Control Appl.*, Vancouver, BC, Canada, 2011, pp. 102–109.
[23] D. Piyabongkarn, R. Rajamani, J. A. Grogg, and J. Y. Lew, "Development and experimental evaluation of a slip angle estimator for vehicle stability control," *IEEE Trans. Control Syst. Technol.*, vol. 17, no. 1, pp. 78–88, Jan. 2009.
[24] G. Phanomchoeng, A. Zemouche, and R. Rajamani, "Real-time automotive slip angle estimation with extended H_∞ circle criterion observer for nonlinear output system," in *Proc. Amer. Control Conf. (ACC)*, Seattle, WA, USA, May 2017, pp. 1636–1641.
[25] C. C. MacAdam, "Application of an optimal preview control for simulation of closed-loop automobile driving," *IEEE Trans. Syst., Man, Cybern.*, vol. SMC-11, no. 6, pp. 393–399, Jun. 1981.
[26] J. Yoon, W. Cho, B. Koo, and K. Yi, "Unified chassis control for rollover prevention and lateral stability," *IEEE Trans. Veh. Technol.*, vol. 58, no. 2, pp. 596–609, Feb. 2009.
[27] J. Edrén, M. Jonasson, J. Jerrelind, A. Stensson Trigell, and L. Drugge, "Utilisation of optimisation solutions to control active suspension for decreased braking distance," *Vehicle Syst. Dyn.*, vol. 53, no. 2, pp. 256–273, Feb. 2015.
[28] A. Kunnappillil Madhusudhanan, M. Corno, and E. Holweg, "Sliding mode-based lateral vehicle dynamics control using tyre force measurements," *Vehicle Syst. Dyn.*, vol. 53, no. 11, pp. 1599–1619, Nov. 2015.
[29] J. Kang, J. Yoo, and K. Yi, "Driving control algorithm for maneuverability, lateral stability, and rollover prevention of 4WD electric vehicles with independently driven front and rear wheels," *IEEE Trans. Veh. Technol.*, vol. 60, no. 7, pp. 2987–3001, Sep. 2011.
[30] X.-H. Chang, Y. Liu, and M. Shen, "Resilient control design for lateral motion regulation of intelligent vehicle," *IEEE/ASME Trans. Mechatronics*, vol. 24, no. 6, pp. 2488–2497, Dec. 2019.
[31] W. Cho, J. Choi, C. Kim, S. Choi, and K. Yi, "Unified chassis control for the improvement of agility, maneuverability, and lateral stability," *IEEE Trans. Veh. Technol.*, vol. 61, no. 3, pp. 1008–1020, Mar. 2012.
[32] S. Zhao, Y. Li, L. Zheng, and S. Lu, "Vehicle lateral stability control based on sliding mode control," in *Proc. IEEE Int. Conf. Autom. Logistics*, Shandong, China, Aug. 2007, pp. 638–642.
[33] R. Rajamani, G. Phanomchoeng, D. Piyabongkarn, and J. Y. Lew, "Algorithms for real-time estimation of individual wheel tire-road friction coefficients," *IEEE/ASME Trans. Mechatronics*, vol. 17, no. 6, pp. 1183–1195, Dec. 2012.
[34] J. Wang and R. G. Longoria, "Coordinated and reconfigurable vehicle dynamics control," *IEEE Trans. Control Syst. Technol.*, vol. 17, no. 3, pp. 723–732, May 2009.
[35] J. J. Burken, P. Lu, Z. Wu, and C. Bahm, "Two reconfigurable flight-control design methods: Robust servomechanism and control allocation," *J. Guid., Control, Dyn.*, vol. 24, no. 3, pp. 482–493, May 2001.
[36] E. Joa, K. Yi, and K. Kim, "A lateral driver model for vehicle–driver closed-loop simulation at the limits of handling," *Vehicle Syst. Dyn.*, vol. 53, no. 9, pp. 1247–1268, Sep. 2015.
[37] J. P. S. Mejia, P. A. Theodosis, and J. C. Gerdes, "Using a path-fitting algorithm to analyze the racing techniques of a skilled driver," in *Proc. ASME Dyn. Syst. Control Conf., Amer. Soc. Mech. Eng. Digit. Collection*, Palo Alto, CA, USA, Oct. 2013, pp. 1–7.
[38] E. Velenis and P. Tsiotras, "Optimal velocity profile generation for given acceleration limits: Theoretical analysis," in *Proc. Amer. Control Conf.*, Jun. 2005, pp. 1478–1483.

JIANBO FENG received the B.S. degree in mechanical engineering from Zhengzhou University, Zhengzhou, China, in 2012. He is currently pursuing the Ph.D. degree in vehicle engineering with the Beijing Institute of Technology. From October 2016 to October 2018, he studied at the Vehicle Dynamics Laboratory, University of California at Berkeley, Berkeley. His research interests include vehicle dynamics control, vehicle chassis dynamics control, and real-time four wheel drive.

SIZHONG CHEN received the M.S. degree from Jilin University, China, in 1987. He is currently a Professor with the School of Mechanical and Vehicular Engineering, Beijing Institute of Technology. His research interests include suspension dynamics and control, steering system design, and vehicle dynamics control. He serves as the Secretary General with the SUV Technology Committee of the Society of Automotive Engineering of China.

ZHIQUAN QI received the Ph.D. degree from the Beijing Institute of Technology, in 2004. He is currently an Associate Professor with the School of Mechanical and Vehicular Engineering, Beijing Institute of Technology. His research interests include vehicle state estimation, vehicle dynamics control, tire model/intelligent model, and auxiliary/pilotless driving.